ACS OMEGA

http://pubs.acs.org/journal/acsodf

Article

Newly Synthesized Pyrazolinone Chalcones as Anticancer Agents via Inhibiting the PI3K/Akt/ERK1/2 Signaling Pathway

Ahmed A. Noser, Ihsan A. Shehadi, Aboubakr H. Abdelmonsef,* and Maha M. Salem

Cite This: *ACS Omega* 2022, 7, 25265−25277

Read Online

ACCESS | Metrics & More | Article Recommendations | Supporting Information

ABSTRACT: A series of novel pyrazolinone chalcones **3**−**9** have been synthesized through the condensation of azo pyrazolinone derivatives with various aromatic aldehydes. Spectroscopic techniques and elemental analysis have both corroborated this. Furthermore, all compounds were screened in silico for their ability to inhibit cancer proliferation and metastasis by targeting the PI3K/Akt signaling pathway. This inhibitory pathway might be an efficient approach for the death of cancer cells, angiogenesis, and metastasis prevention. Our results indicated that only compound **6b** was the top-ranked. It demonstrated the highest binding energies of −11.1 and −10.7 kcal/mol against the target proteins PI3K and Akt, respectively; thus, it was chosen for in vitro studies. Compound **6b** exhibited the most effective cytotoxic impact against the Caco cell line with IC_{50} of 23.34 ± 0.14 μM. Furthermore, it showed significant inhibition of PI3K/Akt proteins and oxidative stress, leading to elevated Bax and p53 expression, reduced Bcl_{-2} expression, and triggered cell cycle arrest at the sub-G0/G1 phase. Additionally, it showed significant downregulation of the Raf-1 gene, leading to ERK1/2 protein inhibition. These findings demonstrate that compound **6b** obeyed Lipinski's rule of five and might be used as a favored scaffold for cancer treatment by inhibiting proliferation and metastasis via inhibition of the PI3K/Akt and Raf-1/ERK1/2 signaling pathways.

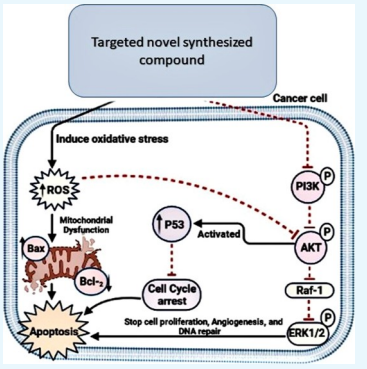

INTRODUCTION

Cancer is a potentially fatal disease that affects people worldwide. The environmental variables account for 90−95% of all cancer cases, with the remaining cases 5−10% attributed to inherited genetic factors. Moreover, surgery, radiation, and chemotherapy were the mainstays of cancer treatment in the past. Even though chemotherapy is the most often used treatment, several chemotherapeutic drugs have harmful side effects, including the indiscriminate death of normal cells and chemotherapeutic resistance.[1] As a result, a constant quest for alternative, targeted, novel, efficacious, and less toxic anticancer agents that inhibit metabolic target proteins are urgently needed. Therefore, designing the bioenergetic drugs that disrupt the metabolic route essential for cancer cell survival, metastasis, and proliferation is of critical importance in this context.[2]

Akt is a proto-oncogenic serine−threonine kinase that plays a role in cell proliferation, glucose metabolism, cell migration, and apoptosis. Akt is activated in tumor cells via phosphorylation, which arises when a PI3K-phosphorylated phosphoinositide (PI) termed PIP3 attaches to the homology Akt domain, followed by translocation to the plasma membrane and phosphorylation by PDK1 and PDK2 at two phosphorylation Ser473 and Thr308 sites. As a result, direct PI3K/Akt

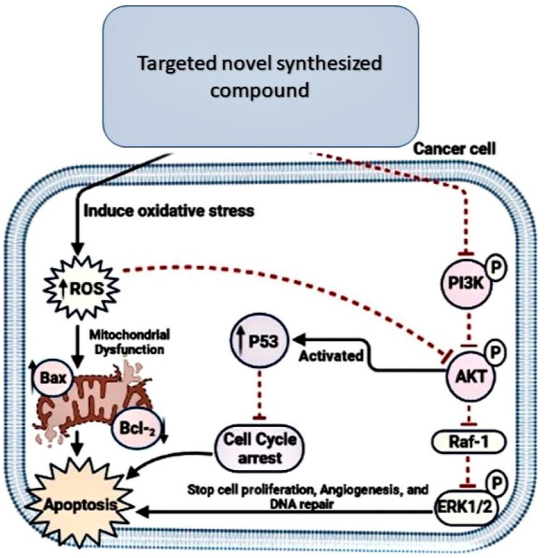

Figure 1. Schematic diagram of the design strategy signaling pathways.

Received: April 7, 2022
Accepted: June 8, 2022
Published: June 27, 2022

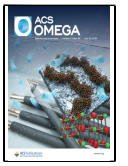

degradation was discovered to inhibit Akt activity and induce apoptosis.[3] For several years, inhibition of Akt has been regarded as a promising therapeutic approach in oncology as it leads to the inhibition of Raf-1, which inhibits the proliferating and angiogenesis proteins, MEK and ERK1/2. Moreover, oxidative stress inhibits the PI3K/Akt signaling pathway and promotes reactive oxygen species (ROS) generation, resulting in Bax and p53 activation, cell cycle arrest, and cancer cell apoptosis.[4] Many efforts have been undertaken to design new anticancer agents that are both selective and effective to inhibit PI3K/Akt and Raf-1/ERK1/2 as they can worsen the proliferation of cancer cells, leading to global programming of cancer cell death and inducing mitochondrial dysfunction because of oxidative stress[5,6] (Figure 1).

Chalcones possess many biological activities, including antibacterial, antifungal, antimalarial, anticonvulsant, and anticancer agents.[7] Furthermore, these compounds are of high interest because of their use in synthesizing many biologically active heterocycles such as azepines, pyrazolines, and flavones.[8−11]

Pyrazolinones have a wide range of biological effects, including anti-inflammatory, antibacterial, antifungal, analgesic, antidiabetic, antioxidant, and anticancer properties. One of the most effective drug-bearing pyrazoline moieties is Axitinib, which is used as an anticancer drug. To create effective anticancer medicines, pyrazoline is also hybridized with other nitrogen-, sulfur-, and oxygen-containing heterocyclic scaffolds such as quinoline, indole, oxazole, and thiazole.[12−14]

This project aimed to design and synthesize novel anticancer scaffolds of pyrazolinone chalcones due to the importance of pyrazolinones and chalcones in the medical area. Computer-based docking experiments were performed on the produced compounds to study the binding mechanism with the active sites of the target enzymes. In addition, in silico physicochemical and pharmacokinetic properties were carried out to estimate the absorption, distribution, metabolism, excretion, and toxicity (ADMET) properties of the compounds as well as investigate the structure−activity relationship (SAR). Ultimately, the chosen compound was investigated in vitro to confirm its inhibitory efficacy toward cancer cell proliferation and metastasis by targeting PI3K/Akt and Raf-1/ERK1/2 signaling pathway inhibition.

MATERIALS AND METHODS

Chemicals and Drugs. Ethyl acetoacetate (EAA), phenylhydrazine, 2,4-dinitrophenylhydrazine (DNP), hydrazine hydrate, *p*-aminoacetophenone, sodium nitrite, benzaldehyde, 3,5-dimethoxybenzaldehyde, 4-(*N*,*N*-dimethylamino)-benzaldehyde, 4-hydroxybenzaldehyde, 2-nitrobenzaldehyde, cinnamaldehyde, 4-(*N*,*N*-dimethylamino)cinnamaldehyde, sodium hydroxide, ethyl alcohol, glacial acetic acid, trichloroacetic acid (TCA), sodium pyrophosphate, reduced glutathione (GSH), and thiobarbituric acid (TBA) were obtained from Sigma-Aldrich Chemical Co. (St. Louis, MO, USA). Doxorubicin HCl injection, USP, was purchased from Pfizer injectables.

General Information. Thin-layer chromatography monitored the reactions performed on precoated Merck Kieselgel 60 F254 plates (EMD Millipore Corporation, Billerica, MA, USA). A PerkinElmer 1420 spectrophotometer (Waltham, MA, USA) was used to record infrared spectra at the Central Laboratory of Tanta University. The KBr disc technique was used to obtain the spectra. The samples were mounted on a sample holder with a big cavity after drying. The open capillary method was used to estimate melting points, which were calculated using the Gallenkamp melting point and reported uncorrected. Electron impact mass spectrometry (EIMS) was used to measure mass spectra at 70 eV at Al-Azhar University's Regional Center for Mycology and Biotechnology. A PerkinElmer 240 CHN Elemental Analyzer was used to undertake elemental analysis of substances at Cairo University's Microanalytical Center. The ^{1}H NMR spectra were recorded on a Bruker AC spectrometer (400 MHz) and ^{13}C NMR (100 MHz at 25 °C in DMSO-d_6 with tetramethylsilane as an internal standard. The chemical shifts for ^{1}H NMR are reported in ppm from tetramethylsilane (0 ppm) or referenced to the solvent (DMSO-d_6, δ2.50). Chemical shifts (δ) for ^{13}C NMR spectra are referenced to the signals for residual deuterated solvents (DMSO-d_6, 37.5). Multiplicities are reported by the following abbreviations: s (singlet), d (doublet), m (multiplet).

*Synthesis of Pyrazolinone Derivatives (**1a−c**).* A mixture of EAA (10 mmol, 1.28 mL) and hydrazine derivatives (10 mmol) in 30 mL of ethanol was refluxed for 18 h, then cooled, filtered, and recrystallized from ethanol to give compounds **1a−c** as described by Alharthy.[15]

*Synthesis of Azo Pyrazolinone Derivatives (**2a−c**).* Azo pyrazolinone derivatives (**2a−c**) were prepared by coupling the pyrazolinone (**1a−c**) with a freshly prepared solution of *p*-acetyl phenyl diazoniumchloride in the presence of aluminum chloride ($AlCl_3$) as described by Khalil.[16]

*4-((4-Acetylphenyl)diazenyl)-3-methyl-1H-pyrazol-5(4H)-one (**2a**).* The structure of **2a** was confirmed as described earlier.[16]

*4-((4-Acetylphenyl) diazenyl)-3-methyl-1-phenyl-1H-pyrazol-5(4H)-one (**2b**).* Reddish-brown powder; yield 91%; mp 129 °C; ^{1}H NMR (400 MHz, DMSO-d_6): δ (ppm) 7.00−7.90 (m, 9H, Ar-H), 2.85 (s, 3H, CH_3−CO), 2.35 (s, 1H, CH), 1.20 (s, 3H, CH_3); ^{13}C NMR (100 MHz, DMSO-d_6): δ (ppm) 198.00, 168.30, 155.9, 155.60, 140.70, 134.00, 129.60, 129.30, 124.70, 122.80, 121.90, 62.20, 29.60, 19.80; IR (KBr) ν: 1500−1560 (N═N), 1670 (CO); EIMS *m*/*z*: 320.15 $[M]^+$ ($C_{18}H_{16}N_4O_2$, calcd 320.35); Anal. Calcd for $C_{18}H_{16}N_4O_2$ (320.35): C, 67.49%; H, 5.03%; N, 17.49%. Found: C, 67.17%; H, 4.91%; N, 17.11%.

*4-((4-Acetylphenyl)diazenyl)-1-(2,4-dinitrophenyl)-3-methyl-1H-pyrazol-5(4H)-one (**2c**).* Reddish-brown powder; yield 89%; mp 89 °C; ^{1}H NMR (400 MHz, DMSO-d_6): δ (ppm) 7.40−9.11 (m, 7H, Ar-H), 2.85 (s, 3H, CH_3−CO), 2.35 (s, 1H, CH), 1.20 (s, 3H, CH_3); ^{13}C NMR (100 MHz, DMSO-d_6): δ (ppm) 198.00, 168.30, 155.9, 155.60, 150.20, 142.30, 141.50, 134.00, 129.60, 127.7, 123.70, 122.80, 111.20, 62.20, 29.60, 19.80; IR (KBr) ν: 1509−1600 (N═N), 1673 (CO); EIMS *m*/*z*: 410.23 $[M]^+$ ($C_{18}H_{14}N_6O_6$, calcd 410.34); Anal. Calcd for $C_{18}H_{14}N_6O_6$ (410.34): C, 52.69%; H, 3.44%; N, 20.48%. Found: C, 52.27%; H, 3.22%; N, 20.18%.

*General Procedure for the Synthesis of Pyrazolinone Chalcones (**3−9**).* In a 50 mL conical flask, a mixture of aromatic aldehyde (1 mmol), azo pyrazolinone derivatives (**2a−c**, 1 mmol), sodium hydroxide (0.08 g, 2 mmol), and ethanol (10.0 mL) was stirred at room temperature for 20 h (TLC control, petroleum ether/ethyl acetate: 8:2). Then the reaction mixture was poured into ice water, filtered off, and dried.

*(E)-4-((4-Cinnamoylphenyl)diazenyl)-3-methyl-1H-pyrazol-5(4H)-one (**3a**).* Reddish-brown powder; yield 91%; mp

https://doi.org/10.1021/acsomega.2c02181
ACS Omega 2022, 7, 25265−25277

174 °C; ^{1}H NMR (400 MHz, DMSO-d_6): δ (ppm) 8.00 (d, 1H, CH-Ph), 7.60 (d, 1H, CH−CO), 6.90 (s, 1H, NH), 7.10−7.80 (m, 9H, Ar-H), 2.35 (s, 1H, CH), 1.20 (s, 3H, CH_3); ^{13}C NMR (100 MHz, DMSO-d_6): δ (ppm) 190.00, 173.30, 157.00, 155.90, 145.50, 135.50, 135.20, 130.70, 129.00, 128.00, 126.70, 123.40, 121.70, 64.80, 19.50; IR (KBr) ν: 1560 (N═N), 1677 (CO); EIMS m/z: 332.16 $[M]^+$ ($C_{19}H_{16}N_4O_2$, calcd 332.36); Anal. Calcd for $C_{19}H_{16}N_4O_2$ (332.36): C, 68.66%; H, 4.85%; N, 16.86%. Found: C, 68.16%; H, 4.65%; N, 16.46%.

*(E)-4-((4-Cinnamoylphenyl)diazenyl)-3-methyl-1-phenyl-1H-pyrazol-5(4H)-one (**3b**).* Reddish-brown powder; yield 92%; mp 112 °C; ^{1}H NMR (400 MHz, DMSO-d_6): δ (ppm) 8.10 (d, 1H, CH-Ph), 7.65 (d, 1H, CH−CO), 7.00−7.80 (m, 14H, Ar-H), 2.35 (s, 1H, CH), 1.20 (s, 3H, CH_3); ^{13}C NMR (100 MHz, DMSO-d_6): δ (ppm) 190.00, 168.30, 157.00, 155.90, 145.50, 140.70, 135.50, 135.20, 132.40, 130.70, 129.30, 129.00, 128.00, 126.70, 124.70, 123.40, 121.90, 121.70, 62.20, 19.80; IR (KBr) ν: 1552 (N═N), 1657 (CO); EIMS m/z: 408.28 $[M]^+$ ($C_{25}H_{20}N_4O_2$, calcd 408.45); Anal. Calcd for $C_{25}H_{20}N_4O_2$ (408.45): C, 73.51%; H, 4.94%; N, 13.72%. Found: C, 73.11%; H, 4.84%; N, 13.44%.

*(E)-4-((4-Cinnamoylphenyl)diazenyl)-1-(2,4-dinitrophenyl)-3-methyl-1H-pyrazol-5(4H)-one (**3c**).* Brown powder; yield 91%; mp 108 °C; ^{1}H NMR (400 MHz, DMSO-d_6): δ (ppm) 7.10−9.05 (m, 12H, Ar-H), 7.90 (d, 1H, CH-Ph), 7.50 (d, 1H, CH−CO), 2.35 (s, 1H, CH), 1.20 (s, 3H, CH_3); ^{13}C NMR (100 MHz, DMSO-d_6): δ (ppm) 190.00, 168.30, 157.00, 155.90, 145.50, 145.20, 142.30, 141.50, 135.50, 135.20, 130.70, 129.00, 128.00, 126.70, 123.70, 123.40, 121.70, 111.20, 62.20, 19.80; IR (KBr) ν: 1570 (N═N), 1666 (CO); EIMS m/z: 498.11 $[M]^+$ ($C_{25}H_{18}N_6O_6$, calcd 498.45); Anal. Calcd for $C_{25}H_{18}N_6O_6$ (498.45): C, 60.24%; H, 3.64%; N, 16.86%. Found: C, 59.98%; H, 3.48%; N, 16.56%.

*(E)-4-((4-(3-(3,5-Dimethoxyphenyl)acryloyl)phenyl)diazenyl)-3-methyl-1H-pyrazol-5(4H)-one (**4a**).* Reddish-brown powder; yield 90%; mp 155 °C; ^{1}H NMR (400 MHz, DMSO-d_6): δ (ppm) 8.05 (d, 1H, CH-Ph), 7.60 (d, 1H, CH−CO), 7.00 (s, 1H, NH), 6.10−7.80 (m, 7H, Ar-H), 3.70 (s, 6H, 2CH_3−O), 2.35 (s, 1H, CH), 1.20 (s, 3H, CH_3); ^{13}C NMR (100 MHz, DMSO-d_6): δ (ppm) 190.00, 173.30, 161.90, 157.00, 155.90, 145.50, 137.50, 135.20, 130.70, 123.40, 121.70, 103.20, 99.90, 70.70, 56.20, 19.50; IR (KBr) ν: 1451 (N═N), 1598 (CO), 2931 (OMe); EIMS m/z: 392.19 $[M]^+$ ($C_{21}H_{20}N_4O_4$, calcd 392.41); Anal. Calcd for $C_{21}H_{20}N_4O_4$ (392.41): C, 64.28%; H, 5.14%; N, 14.28%. Found: C, 63.98%; H, 4.98%; N, 14.08%.

*(E)-4-((4-(3-(3,5-Dimethoxyphenyl)acryloyl)phenyl)diazenyl)-3-methyl-1-phenyl-1H-pyrazol-5(4H)-one (**4b**).* Reddish-brown powder; yield 89%; mp 172 °C; ^{1}H NMR (400 MHz, DMSO-d_6): δ (ppm) 8.05 (d, 1H, CH-Ph), 7.60 (d, 1H, CH−CO), 6.30−7.80 (m, 12H, Ar-H), 3.70 (s, 6H, 2CH_3−O), 2.35 (s, 1H, CH), 1.20 (s, 3H, CH_3); ^{13}C NMR (100 MHz, DMSO-d_6): δ (ppm) 190.00, 168.30, 161.90, 157.00, 155.90, 145.50, 140.60, 137.50, 135.20, 130.70, 129.30, 124.70, 123.40, 121.90, 121.70, 103.20, 99.90, 62.20, 56.20, 19.80; IR (KBr) ν: 1595 (N═N), 1655 (CO), 2837 (OMe); EIMS m/z: 468.37 $[M]^+$ ($C_{27}H_{24}N_4O_4$, calcd 468.50); Anal. Calcd for $C_{27}H_{24}N_4O_4$ (468.50): C, 69.22%; H, 5.16%; N, 11.96%. Found: C, 68.98%; H, 5.02%; N, 11.86%.

*(E)-4-((4-(3-(3,5-Dimethoxyphenyl)acryloyl)phenyl)diazenyl)-1-(2,4-dinitrophenyl)-3-methyl-1H-pyrazol-5(4H)-one (**4c**).* Brown powder; yield 90%; mp 154 °C; ^{1}H NMR (400 MHz, DMSO-d_6): δ (ppm) 7.95 (d, 1H, CH-Ph), 7.65 (d, 1H, CH−CO), 6.30−9.10 (m, 10H, Ar-H), 3.70 (s, 6H, 2CH_3−O), 2.35 (s, 1H, CH), 1.20 (s, 3H, CH_3); ^{13}C NMR (100 MHz, DMSO-d_6): δ (ppm) 190.00, 168.30, 161.90, 155.90, 145.50, 145.20,142.30, 137.50, 135.20, 127.70, 123.70, 121.70, 103.20, 99.90, 62.20, 56.20, 19.80; IR (KBr) ν: 1580 (N=N), 1670 (CO), 2857 (OMe); EIMS m/z: 558.38 $[M]^+$ ($C_{27}H_{22}N_6O_4$, calcd 558.50); Anal. Calcd for $C_{27}H_{22}N_6O_4$ (558.50): C, 58.06%; H, 3.97%; N, 15.05%. Found: C, 57.86%; H, 3.77%; N, 14.91%.

*(E)-4-((4-(3-(4-(Dimethylamino)phenyl)acryloyl)phenyl)diazenyl)-3-methyl-1H-pyrazol-5(4H)-one (**5a**).* Reddish-brown powder; yield 91%; mp 149 °C; ^{1}H NMR (400 MHz, DMSO-d_6): δ (ppm) 8.05 (d, 1H, CH-Ph), 7.60 (d, 1H, CH−CO), 7.00 (s, 1H, NH), 6.50−7.80 (m, 8H, Ar-H), 2.85 (s, 6H, (CH_3)$_2$−N), 2.35 (s, 1H, CH), 1.20 (s, 3H, CH_3); ^{13}C NMR (100 MHz, DMSO-d_6): δ (ppm) 190.00, 173.30, 157.00, 155.90, 149.10, 145.50, 135.20, 130.70, 127.70, 125.00, 123.40, 121.70, 114.50, 64.80, 40.60, 19.50; IR (KBr) ν: 1580 (N═N), 1670 (CO), 1179 (C−N); EIMS m/z: 375.24 $[M]^+$ ($C_{21}H_{21}N_5O_2$, calcd 375.42); Anal. Calcd for $C_{21}H_{21}N_5O_2$ (375.42): C, 67.18%; H, 5.64%; N, 18.65%. Found: C, 67.08%; H, 5.48%; N, 18.53%.

*(E)-4-((4-(3-(4-(Dimethylamino)phenyl)acryloyl)phenyl)diazenyl)-3-methyl-1-phenyl-1H-pyrazol-5(4H)-one (**5b**).* Reddish-brown powder; yield 91%; mp 214 °C; ^{1}H NMR (400 MHz, DMSO-d_6): δ (ppm) 8.05 (d, 1H, CH-Ph), 7.60 (d, 1H, CH−CO), 6.50−7.80 (m, 13H, Ar-H), 2.90 (s, 6H, (CH_3)$_2$−N), 2.35 (s, 1H, CH), 1.20 (s, 3H, CH_3); ^{13}C NMR (100 MHz, DMSO-d_6): δ (ppm) 190.00, 168.30, 157.00, 155.90, 149.10, 145.50, 140.70, 135.20, 130.70, 129.30, 127.60, 125.00, 124.20, 123.40, 121.90, 121.70, 114.50, 62.20, 40.60, 19.80; IR (KBr) ν: 1562 (N═N), 1653 (CO), 1159 (C−N); EIMS m/z: 451.32 $[M]^+$ ($C_{27}H_{25}N_5O_2$, calcd 451.52); Anal. Calcd for $C_{27}H_{25}N_5O_2$ (451.52): C, 71.82%; H, 5.58%; N, 15.51%. Found: C, 71.62%; H, 5.46%; N, 15.31%.

*(E)-4-((4-(3-(4-(Dimethylamino)phenyl)acryloyl)phenyl)diazenyl)-1-(2,4-dinitrophenyl)-3-methyl-1H-pyrazol-5(4H)-one (**5c**).* Brown powder; yield 92%; mp 134 °C; ^{1}H NMR (400 MHz, DMSO-d_6): δ (ppm) 7.95 (d, 1H, CH-Ph), 7.65 (d, 1H, CH−CO), 6.50−9.10 (m, 11H, Ar-H), 2.85 (s, 6H, (CH_3)$_2$−N), 2.35 (s, 1H, CH), 1.20 (s, 3H, CH_3); ^{13}C NMR (100 MHz, DMSO-d_6): δ (ppm) 190.00, 168.30, 157.00, 155.90, 149.10, 145.20, 145.50, 142.30, 141.50, 135.20, 130.70, 127.70, 127.60, 125.00, 123.70, 123.40, 121.70, 119.20, 114.50, 62.20, 40.60, 19.80; IR (KBr) ν: 1570 (N═N), 1655 (CO), 1165 (C−N); EIMS m/z: 541.07 $[M]^+$ ($C_{27}H_{23}N_7O_6$, calcd 541.17); Anal. Calcd for $C_{27}H_{23}N_7O_6$ (541.17): C, 59.89%; H, 4.28%; N, 18.11%. Found: C, 59.49%; H, 4.16%; N, 17.95%.

*(E)-4-((4-(3-(4-Hydroxyphenyl)acryloyl)phenyl)diazenyl)-3-methyl-1H-pyrazol-5(4H)-one (**6a**).* Reddish-brown powder; yield 92%; mp 202 °C; ^{1}H NMR (400 MHz, DMSO-d_6): δ (ppm) 8.05 (d, 1H, CH-Ph), 7.60 (d, 1H, CH−CO), 7.00 (s, 1H, NH), 6.50−7.80 (m, 8H, Ar-H), 5.00 (s, 1H, OH), 2.35 (s, 1H, CH), 1.20 (s, 3H, CH_3); ^{13}C NMR (100 MHz, DMSO-d_6): δ (ppm) 190.00, 173.30, 158.00, 157.00, 155.90, 145.50, 135.20, 130.70, 128.10, 123.40, 121.70, 116.10, 64.80, 19.50; IR (KBr) ν: 1385 (N═N), 1641 (CO), 3457 (OH); EIMS m/z: 348.23 $[M]^+$ ($C_{19}H_{16}N_4O_3$, calcd 348.36); Anal. Calcd for $C_{19}H_{16}N_4O_3$ (348.36): C, 65.51%; H, 4.63%; N, 16.08%. Found: C, 65.33%; H, 4.43%; N, 15.94%.

*(E)-4-((4-(3-(4-Hydroxyphenyl)acryloyl)phenyl)diazenyl)-3-methyl-1-phenyl-1H-pyrazol-5(4H)-one (**6b**).* Reddish-brown powder; yield 93%; mp 193 °C; ^{1}H NMR (400 MHz,

https://doi.org/10.1021/acsomega.2c02181
ACS Omega 2022, 7, 25265−25277

DMSO-d_6): δ (ppm) 8.05 (d, 1H, CH-Ph), 7.60 (d, 1H, CH−CO), 6.50−7.80 (m, 13H, Ar-H), 5.00 (s, 1H, OH), 2.35 (s, 1H, CH), 1.20 (s, 3H, CH_3); ^{13}C NMR (100 MHz, DMSO-d_6): δ (ppm) 190.00, 168.30, 158.00, 157.00, 155.90, 145.50, 140.70, 135.20, 130.70, 129.30, 124.70, 121.90, 116.10, 62.20, 19.80; IR (KBr) ν: 1559 (N═N), 1664 (CO), 3166 (OH); EIMS m/z: 424.32 $[M]^+$ ($C_{25}H_{20}N_4O_3$, calcd 424.45); Anal. Calcd for $C_{25}H_{20}N_4O_3$ (424.45): C, 70.74%; H, 4.75%; N, 13.20%. Found: C, 70.44%; H, 4.55%; N, 13.08%.

*(E)-1-(2,4-Dinitrophenyl)-4-((4-(3-(4-hydroxyphenyl)-acryloyl)phenyl)diazenyl)-3-methyl-1H-pyrazol-5(4H)-one (**6c**).* Brown powder; yield 92%; mp 124 °C; ^{1}H NMR (400 MHz, DMSO-d_6): δ (ppm) 7.95 (d, 1H, CH-Ph), 7.65 (d, 1H, CH−CO), 6.50−9.10 (m, 11H, Ar-H), 5.00 (s, 1H, OH), 2.35 (s, 1H, CH), 1.20 (s, 3H, CH_3); ^{13}C NMR (100 MHz, DMSO-d_6): δ (ppm) 190.00, 168.30, 158.00, 157.00, 155.90, 145.50, 145.20, 142.30, 141.50, 135.20, 130.70, 128.10, 127.70, 123.70, 123.40, 121.70, 119.20, 116.10, 62.20, 19.80; IR (KBr) ν: 1560 (N═N), 1671 (CO), 3240 (OH); EIMS m/z: 514.25 $[M]^+$ ($C_{25}H_{18}N_6O_7$, calcd 514.45); Anal. Calcd for $C_{25}H_{18}N_6O_7$ (514.45): C, 58.37%; H, 3.53%; N, 16.34%. Found: C, 58.17%; H, 3.23%; N, 16.22%.

*(E)-3-Methyl-4-((4-(3-(2-nitrophenyl)acryloyl)phenyl)-diazenyl)-1H-pyrazol-5(4H)-one (**7a**).* Reddish-brown powder; yield 93%; mp 175 °C; ^{1}H NMR (400 MHz, DMSO-d_6): δ (ppm) 8.50 (d, 1H, CH-Ph), 7.60 (d, 1H, CH−CO), 7.00 (s, 1H, NH), 7.40−8.00 (m, 8H, Ar-H), 2.35 (s, 1H, CH), 1.20 (s, 3H, CH_3); ^{13}C NMR (100 MHz, DMSO-d_6): δ (ppm) 190.00, 173.30, 157.00, 155.90, 146.40, 135.20, 135.10, 130.70, 130.30, 129.20, 127.50, 123.40, 121.70, 121.30, 64.80, 19.50; IR (KBr) ν: 1580 (N═N), 1690 (CO), 1490−1520 (N−O); EIMS m/z: 377.25 $[M]^+$ ($C_{19}H_{15}N_5O_4$, calcd 377.35); Anal. Calcd for $C_{19}H_{15}N_5O_4$ (377.35): C, 60.47%; H, 4.01%; N, 18.56%. Found: C, 60.27%; H, 3.93%; N, 18.44%.

*(E)-3-Methyl-4-((4-(3-(2-nitrophenyl)acryloyl)phenyl)-diazenyl)-1-phenyl-1H-pyrazol-5(4H)-one (**7b**).* Reddish-brown powder; yield 91%; mp 135 °C; ^{1}H NMR (400 MHz, DMSO-d_6): δ (ppm) 8.50 (d, 1H, CH-Ph), 7.60 (d, 1H, CH−CO), 7.40−8.00 (m, 13H, Ar-H), 2.35 (s, 1H, CH), 1.20 (s, 3H, CH_3); ^{13}C NMR (100 MHz, DMSO-d_6): δ (ppm) 190.00, 168.30, 157.00, 155.90, 146.40, 145.50, 140.70, 135.20, 135.10, 130.70, 130.30, 129.30, 129.20, 127.50, 124.70, 123.40, 121.90, 121.70, 121.30, 62.20, 19.80; IR (KBr) ν: 1570 (N═N), 1680 (CO), 1480−1515 (N−O); EIMS m/z: 453.22 $[M]^+$ ($C_{25}H_{19}N_5O_4$, calcd 453.45); Anal. Calcd for $C_{25}H_{19}N_5O_4$ (453.45): C, 66.22%; H, 4.22%; N, 15.44%. Found: C, 66.10%; H, 4.08%; N, 15.26%.

*(E)-1-(2,4-Dinitrophenyl)-3-methyl-4-((4-(3-(2-nitrophenyl)acryloyl)phenyl)diazenyl)-1H-pyrazol-5(4H)-one (**7c**).* Brown powder; yield 90%; mp 145 °C; ^{1}H NMR (400 MHz, DMSO-d_6): δ (ppm) 8.50 (d, 1H, CH-Ph), 7.65 (d, 1H, CH−CO), 7.40−9.10 (m, 11H, Ar-H), 2.35 (s, 1H, CH), 1.20 (s, 3H, CH_3); ^{13}C NMR (100 MHz, DMSO-d_6): δ (ppm) 190.00, 168.30, 157.00, 155.90, 146.40, 145.50, 145.20, 142.30, 141.50, 135.20, 135.10, 130.70, 130.30, 129.20, 127.70, 127.60, 123.70, 123.40, 121.70, 121.30, 119.20, 62.20, 19.80; IR (KBr) ν: 1560 (N═N), 1670 (CO), 1470−1530 (N−O); EIMS m/z: 543.28 $[M]^+$ ($C_{25}H_{17}N_7O_8$, calcd 543.44); Anal. Calcd for $C_{25}H_{17}N_7O_8$ (543.44): C, 55.25%; H, 3.15%; N, 18.04%. Found: C, 55.13%; H, 3.05%; N, 17.94%.

*3-Methyl-4-((4-((2E,4E)-5-phenylpenta-2,4-dienoyl)-phenyl)diazenyl)-1H-pyrazol-5(4H)-One (**8a**).* Reddish-brown powder; yield 92%; mp 182 °C; ^{1}H NMR (400 MHz, DMSO-d_6): δ (ppm) 7.90 (t, 1H, CH═CH−CO), 7.30 (d, 1H, CH═CH−CO), 7.00 (s, 1H, NH), 7.10−7.70 (m, 9H, Ar-H), 6.85 (t, 1H, CH═CH−Ph), 6.70 (d, 1H, CH═CH−Ph), 2.35 (s, 1H, CH), 1.20 (s, 3H, CH_3); ^{13}C NMR (100 MHz, DMSO-d_6): δ (ppm) 190.00, 173.30, 157.00, 155.90, 144.70, 135.50, 135.20, 131.50, 130.70, 129.30, 129.00, 128.30, 126.70, 125.60, 123.40, 70.70, 19.50; IR (KBr) ν: 1552 (N═N), 1668 (CO), 2930 (═C−H); EIMS m/z: 358.29 $[M]^+$ ($C_{21}H_{18}N_4O_2$, calcd 358.39); Anal. Calcd for $C_{21}H_{18}N_4O_2$ (358.39): C, 70.38%; H, 5.06%; N, 15.63%. Found: C, 70.22%; H, 4.96%; N, 15.45%.

*3-Methyl-1-phenyl-4-((4-((2E,4E)-5-phenylpenta-2,4-dienoyl)phenyl)diazenyl)-1H-pyrazol-5(4H)-one (**8b**).* Reddish-brown powder; yield 92%; mp 136 °C; ^{1}H NMR (400 MHz, DMSO-d_6): δ (ppm) 7.90 (t, 1H, CH═CH−CO), 7.20 (d, 1H, CH═CH−CO), 7.00−7.75 (m, 14H, Ar-H), 6.85 (t, 1H, CH═CH−Ph), 6.70 (d, 1H, CH═CH−Ph), 2.35 (s, 1H, CH), 1.20 (s, 3H, CH_3); ^{13}C NMR (100 MHz, DMSO-d_6): δ (ppm) 190.00, 168.30, 157.00, 155.90, 144.70, 140.70, 135.50, 135.20, 131.50, 130.70, 129.30, 129.00, 128.30, 126.70, 125.60, 124.70, 123.40, 121.90, 68.20, 19.80; IR (KBr) ν: 1572 (N═N), 1688 (CO), 2920 (═C−H); EIMS m/z: 434.29 $[M]^+$ ($C_{27}H_{22}N_4O_2$, calcd 434.49); Anal. Calcd for $C_{27}H_{22}N_4O_2$ (434.49): C, 74.64%; H, 5.10%; N, 12.89%. Found: C, 74.44%; H, 4.98%; N, 12.77%.

*1-(2,4-Dinitrophenyl)-3-methyl-4-((4-((2E,4E)-5-phenyl-penta-2,4-dienoyl)phenyl)diazenyl)-1H-pyrazol-5(4H)-one (**8c**).* Reddish-brown powder; yield 94%; mp 117 °C; ^{1}H NMR (400 MHz, DMSO-d_6): δ (ppm) 7.90 (t, 1H, CH═CH−CO), 7.20 (d, 1H, CH═CH−CO), 7.10−9.10 (m, 12H, Ar-H), 6.85 (t, 1H, CH═CH−Ph), 6.67 (d, 1H, CH═CH−Ph), 2.35 (s, 1H, CH), 1.20 (s, 3H, CH_3); ^{13}C NMR (100 MHz, DMSO-d_6): δ (ppm) 190.00, 168.30, 157.00, 155.90, 145.20, 144.70, 142.30, 141.50, 135.50, 135.20, 131.50, 130.70, 129.30, 129.00, 128.30, 127.70, 126.70, 125.60, 123.70, 123.40, 119.20, 68.20, 19.80; IR (KBr) ν: 1562 (N═N), 1678 (CO), 2918 (═C−H); EIMS m/z: 524.32 $[M]^+$ ($C_{27}H_{20}N_6O_6$, calcd 524.48); Anal. Calcd for $C_{27}H_{20}N_6O_6$ (524.48): C, 61.83%; H, 3.84%; N, 16.02%. Found: C, 61.67%; H, 3.72%; N, 15.92%.

*4-((4-((2E,4E)-5-(4-(Dimethylamino)phenyl)penta-2,4-dienoyl)phenyl)diazenyl)-3-methyl-1H-pyrazol-5(4H)-one (**9a**).* Reddish-brown powder; yield 89%; mp 165 °C; ^{1}H NMR (400 MHz, DMSO-d_6): δ (ppm) 8.05 (t, 1H, CH═CH−CO), 7.65 (d, 1H, CH═CH−CO), 7.00 (s, 1H, NH), 6.35−7.85 (m, 8H, Ar-H), 6.80 (t, 1H, CH═CH−Ph), 6.60 (d, 1H, CH═CH−Ph), 2.85 (s, 6H, $(CH_3)_2$−N), 2.35 (s, 1H, CH), 1.20 (s, 3H, CH_3); ^{13}C NMR (100 MHz, DMSO-d_6): δ (ppm) 190.00, 173.30, 157.00, 155.90, 149.20, 144.70, 135.20, 131.50, 130.70, 127.60, 125.60, 125.00, 123.40, 114.50, 70.80, 40.60, 19.50; IR (KBr) ν: 1570 (N═N), 1660 (CO), 1189 (C−N), 2915 (═C−H); EIMS m/z: 401.26 $[M]^+$ ($C_{23}H_{23}N_5O_2$, calcd 401.46); Anal. Calcd for $C_{23}H_{23}N_5O_2$ (401.46): C, 68.81%; H, 5.77%; N, 17.44%. Found: C, 68.65%; H, 5.55%; N, 17.24%.

*4-((4-((2E,4E)-5-(4-(Dimethylamino)phenyl)penta-2,4-dienoyl)phenyl)diazenyl)-3-methyl-1-phenyl-1H-pyrazol-5(4H)-one (**9b**).* Reddish-brown powder; yield 88%; mp 209 °C; ^{1}H NMR (400 MHz, DMSO-d_6): δ (ppm) 8.00 (t, 1H, CH═CH−CO), 7.60 (d, 1H, CH═CH−CO), 6.50−7.80 (m, 13H, Ar-H), 6.80 (t, 1H, CH═CH−Ph), 6.60 (d, 1H, CH═CH−Ph), 2.85 (s, 6H, $(CH_3)_2$−N), 2.35 (s, 1H, CH), 1.20 (s, 3H, CH_3); ^{13}C NMR (100 MHz, DMSO-d_6): δ (ppm) 190.00, 168.30, 157.00, 155.90, 149.10, 144.70, 140.70, 135.20, 131.50, 130.70, 129.30, 127.70, 125.60, 125.00, 124.70, 123.40, 121.90, 114.50, 68.20, 40.60, 19.80; IR (KBr) ν: 1560 (N═N), 1665

https://doi.org/10.1021/acsomega.2c02181
ACS Omega 2022, 7, 25265−25277

Table 1. Primer Sequences Used in qRT-PCR

gene	forward primer (/5---/3)	reverse primer (/5---/3)
Raf-1	GCAGGATAACAACCCATTC	GGTCAGCGTGCAAGCATT
P53	TAACAGTTCCTGCATGGGCGGC	AGGACAGGCACAAACACGCACC
Bax	GGCTGGACACTGGACTTCCT	GGTGAGGACTCCAGCCACAA
Bcl_{-2}	TTCGCAGAGATGTCCAGTCA	TTCAGAGACAGCCAGGAGAA
GAPDH	TGTGTCCGTCGTGGATCTGA	CCTGCTTCACCACCTTCTTGA

(CO), 1182 (C−N), 2925 (=C−H); EIMS m/z: 477.38 $[M]^+$ ($C_{29}H_{27}N_5O_2$, calcd 477.56); Anal. Calcd for $C_{29}H_{27}N_5O_2$ (477.56): C, 72.94%; H, 5.70%; N, 14.66%. Found: C, 72.78%; H, 5.52%; N, 14.48%.

*4-((4-((2E,4E)-5-(4-(Dimethylamino)phenyl)penta-2,4-dienoyl)phenyl)diazenyl)-1-(2,4-dinitrophenyl)-3-methyl-1H-pyrazol-5(4H)-one (**9c**).* Reddish-brown powder; yield 88%; mp over 300 °C; ^{1}H NMR (400 MHz, DMSO-d_6): δ (ppm) 7.95 (t, 1H, CH=CH−CO), 7.65 (d, 1H, CH=CH−CO), 6.50−9.10 (m, 11H, Ar-H), 6.90 (t, 1H, CH=CH−Ph), 6.70 (d, 1H, CH=CH−Ph), 2.90 (s, 6H, $(CH_3)_2$−N), 2.35 (s, 1H, CH), 1.20 (s, 3H, CH_3); ^{13}C NMR (100 MHz, DMSO-d_6): δ (ppm) 190.00, 168.30, 157.00, 155.90, 149.10, 145.20, 144.70, 142.30, 141.50, 135.20, 131.50, 130.70, 129.30, 127.70, 127.60, 125.60, 125.00, 123.70, 123.40, 119.20, 114.50, 68.20, 40.60, 19.80; IR (KBr) ν: 1565 (N=N), 1680 (CO), 1179 (C−N), 2935 (=C−H); EIMS m/z: 567.39 $[M]^+$ ($C_{29}H_{25}N_7O_6$, calcd 567.55); Anal. Calcd for $C_{29}H_{25}N_7O_6$ (567.55): C, 61.37%; H, 4.44%; N, 17.28%. Found: C, 61.19%; H, 4.26%; N, 17.12%.

In Silico Study. In the current research, molecular docking studies[17−24] were performed to explore the binding modes of the ligand molecules toward the target proteins PI3K and Akt. The crystal structures of the targets were retrieved from the RCSB protein data bank.[25] The target files were optimized by removing the co-crystalized ligands, heteroatoms, and water molecules. In addition, their energies were minimized using CHARM Force Field[26] in Discovery Studio 3.5 Visualizer. Further, the 2D structures of the prepared analogues were generated in cdx format (2D structures) using ChemDraw Ultra 8.0 and then converted to sdf files (3D structures) using the Open Babel GUI 2.4.1 tool.[27] Furthermore, the UFF force field[28] in the PyRx tool was used to minimize their energies. An in-house library of 12 ligand molecules was generated for the docking. The in silico docking technique was performed using PyRx—a virtual screening tool.[29] Grid maps of 25 × 25 × 25 Å^3 were generated around the active site region of the target proteins, resulting in nine conformers for each docked molecule, and the minimum binding energy was selected for further study. The 2D and 3D representations of docking results were visualized using Discovery Studio 3.5. Finally, the drug-like properties of the newly prepared molecules were calculated using mol inspiration, Swiss ADME, and Admet SAR web tools.

Anticancer Investigations on the Expected Compound (In Vitro). The anticancer impact was studied using the tetrazolium 3-(4,5-dimethylthiazol-2-yl)-2,5-diphenyl-tetrazolium bromide (MTT) assay on the most effective compound resulting from the in silico studies and then submitted to further analyses.

Cell Line Maintenance and Treatment. The lung cancer cell line (A549), triple-negative breast cancer cell line (MDA-231), pancreatic cancer cell line (PCL), estrogen receptor-positive breast cancer cell line (MCF-7), colon cancer cell line

Scheme 1. Synthesis Pathway of Compounds 1 and 2

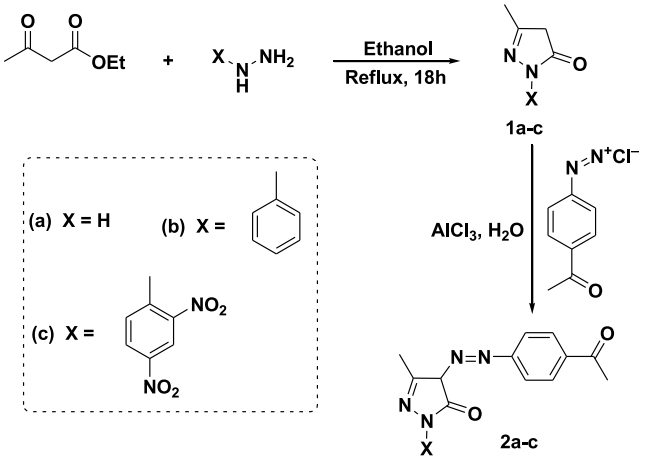

(Caco), and WISH normal cell line were seeded with (1×10^4 cells/well) separately using complete media containing (Dulbecco's modified Eagle's medium with 10% fetal bovine serum and 1% penicillin/streptomycin) in a 5% CO_2 incubator and a 95% humidified environment at 37 °C. All cell lines were provided by the Center of Excellence for Research in Regenerative Medicine and Its Applications, Alexandria University, Egypt. The cell lines were incubated with the selected compound at several concentrations (0−200 μM) and doxorubicin (DOX) as a standard chemotherapeutic drug (0−100 μM) for 48 h, and then, the viability of the cells was determined using the MTT assay (Gibco-BRL, New York, NY, USA).[30,31]

Cell Morphology Study. Briefly, 1×10^5 of the Caco cell line was seeded in a six-well plate, incubated for 24 h, and then treated dose-dependently with $1/4IC_{50}$, $1/2IC_{50}$, and IC_{50} of the selected compound. After 48 h incubation, morphological alterations of treated and untreated cells were evaluated and captured using an inverted light microscope (Olympus, USA).

Cell Cycle Examination. Flow cytometry was used to analyze cell cycle phases using an Accuri C6 flow cytometer (Becton Dickinson BD, USA) on Caco cells 1×10^5 that were trypsinized, centrifuged at 5000 rpm, then washed with 1× cold phosphate-buffered saline (PBS), and fixed with cold absolute ethanol as described by Noser et al. and Darzynkiewicz et al.[31,32]

qPCR Assessment. The Caco 1×10^5 control and treated cells were trypsinized, centrifuged at 4500 rpm, and washed with 1× PBS. Then the pelleted Caco cells were subjected to RNA extraction and transcription to cDNA as described by Kvastad et al.[33] The expression of Raf-1, p53, Bax, and Bcl_{-2} mRNA was measured using Applied qPCR Biosystems (Foster City, USA) on treated and control Caco cells according to Livak and Schmittgen.[34] The primer sequences were designed using primer 3plus as in Table 1.

https://doi.org/10.1021/acsomega.2c02181
ACS Omega 2022, 7, 25265−25277

Scheme 2. Synthesis Pathway of Compounds 3−9

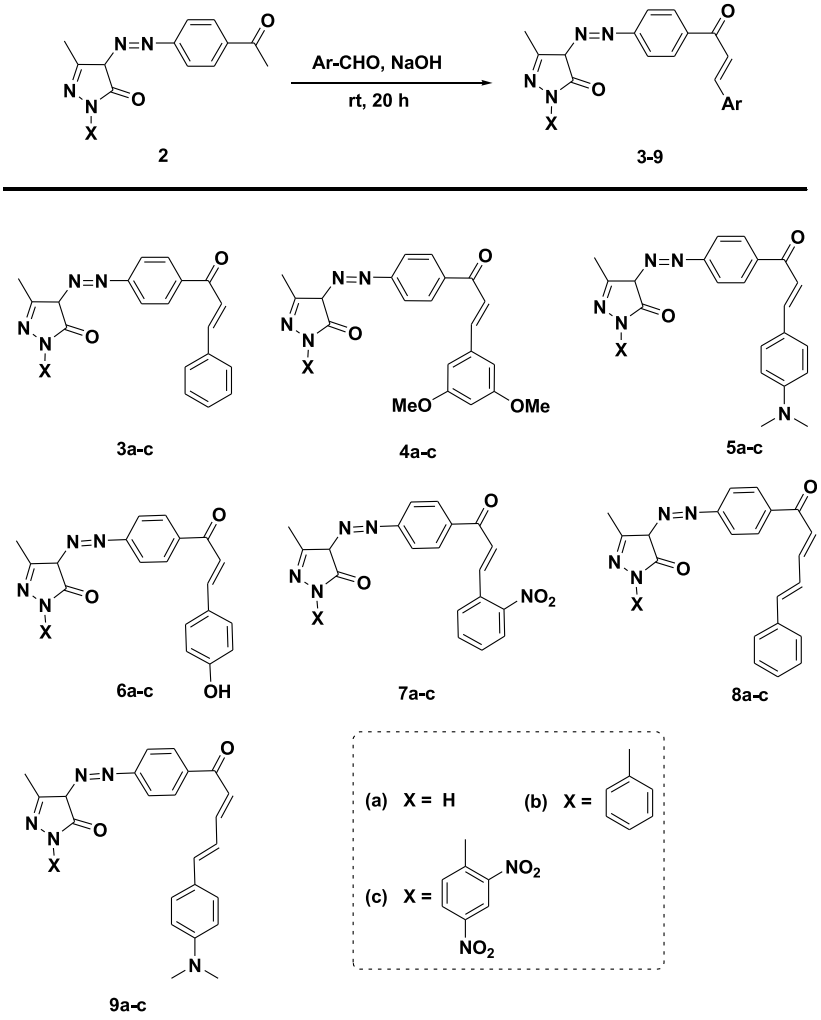

Biomarker Estimation of Antioxidant/Oxidative Stress. The 1×10^5 Caco cells were treated for 48 h. Subsequently, the cells were scraped, and pelleted cells were washed twice with 1× cold PBS. The scraped pelleted cells were incubated in the lysis buffer as described by Noser et al.[31] to measure the levels of malondialdehyde (MDA) and the activity of reduced glutathione (GSH).[35] The protein content was determined using Bradford.[36]

Western Blot Analysis. The method of Mruk and Cheng[37] was used for immunoblotting. Proteins are removed from Caco control and treated cells using cold RIPA lysis buffer and quantified using Bradford.[36] Equal amounts of proteins (20 μg) were separated and transferred to a polyvinylidene difluoride (PVDF) membrane. After blocking the membrane, the primary antibodies as phospho-PI3K (ab182651), phospho-Akt (ab81283), and phospho-ERK1/2 (ab214362) were added and incubated with it. Then, the primary antibodies were removed, carefully washed several times, and incubated with the secondary antibody horseradish peroxidase (HRP)-conjugated goat anti-rabbit IgG (H + L) (ab205718). The bands were visualized and normalized with β-actin as described by Noser et al.[31]

Statistical Analysis. The experimental results are presented as mean ± SE. GraphPad Prism 6 software was used to determine the significance of differences between the control and treated groups using one and two-way ANOVA.

RESULTS AND DISCUSSION

Chemistry of the Synthesized Compounds. The reaction of EAA with hydrazine derivatives led to the formation of pyrazolinone derivatives (**1a−c**) with high yields as described by Alharthy.[15] *p*-Acetyl phenyl diazonium chloride was coupled with the pyrazolinone derivatives (**1a−c**) to give the azo pyrazolinone derivatives (**2a−c**) with 92, 91, and 89% yields, respectively, as described in Scheme 1.

The chalcones (**3−9**) were synthesized from the reaction of azo pyrazolinone derivatives (**2a−c**) with different substituted aromatic aldehydes in a basic medium as described in Scheme 2.

All synthesized compounds **2−9** were characterized using different spectroscopic techniques and elemental analysis.

In Silico Docking Study. PI3K/Akt is one of the major signaling pathways associated with tumor proliferation in human cancer.[38] Therefore, these proteins are selected as pivotal therapeutic targets for identifying cancer agents. In the present study, the molecular docking approach was achieved to explore new PI3K/Akt drug candidates. The screened compounds exhibited docking scores between −8.3 and −11.1 kcal/mol and between −8.6 and −10.7 kcal/mol against PI3K and Akt targets, respectively. The molecular docking studies resulted in compound **6b** having the highest binding energy against the proteins. Figure 2 shows the 2D and 3D

https://doi.org/10.1021/acsomega.2c02181
ACS Omega 2022, 7, 25265−25277

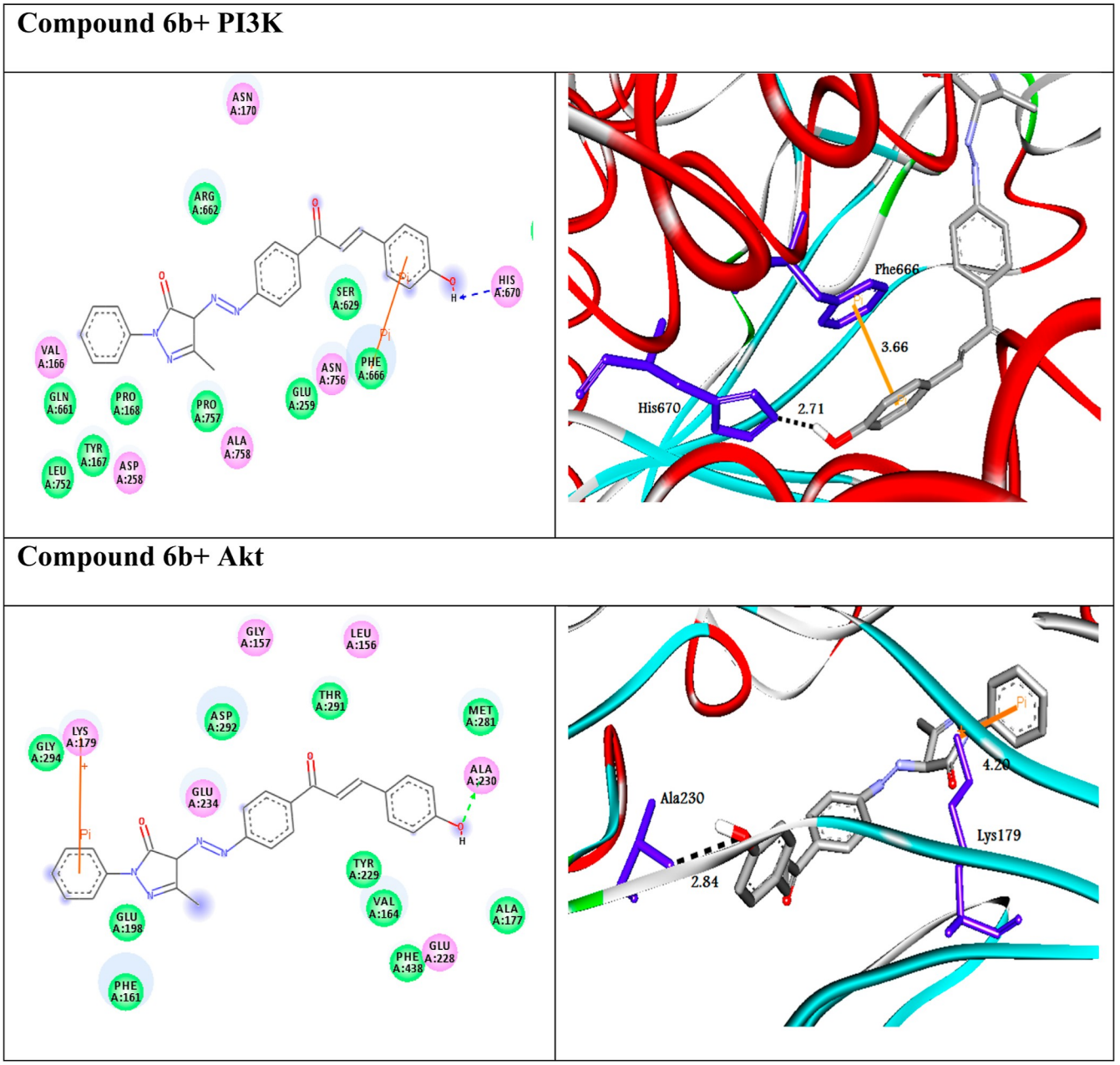

Figure 2. (Left side) 2D and (right side) 3D representations of interactions of the best-docked compound **6b** with amino acid residues of the targets PI3K and Akt.

Table 2. Calculated Docking Scores (in kcal/mol) of the Best-Docked Compound with the Targets

	PI3K			Akt		
compounds	docking score (ΔG_{bind})	docked complex (amino acid–ligand) interactions	distance (Å)	docking score (ΔG_{bind})	docked complex (amino acid–ligand) interactions	distance (Å)
6b	−11.1	H-bond		−10.7	H-bond	
		Asn114---compound **6b**	2.99		Thr195:OG1---compound **6b**	2.12
		Val125---compound **6b**	2.98		Thr195:OG1---compound **6b**	2.98
		Cys126---compound **6b**	2.95		Thr195:OG1---compound **6b**	2.84
		Glu78:OE1---compound **6b**	2.44		Ala230:N---compound **6b**	2.79
		Ser690:OG---compound **6b**	2.71		Glu228:O---compound **6b**	2.35
		π-cation			π-cation	
		Arg140:NH1---compound **6b**	5.86		Lys179:NZ---compound **6b**	4.20
		Arg693:NH2---compound **6b**	4.17			

https://doi.org/10.1021/acsomega.2c02181
ACS Omega 2022, 7, 25265−25277

Table 3. ADMET and Drug-likeness Profiles of the Compounds

	molecular weight (g/mol)	blood−brain barrier (BBB+)	Caco-2 permeability (Caco2+)	% human intestinal absorption (HIA+)	TPSA A^2	logp	HBA	HBD	N rotatable	N violations	GI absorption	carcinogenicity
acceptable ranges	130−500	−3 to 1.2	<25 poor, 500 great	<80% high, >25% low	≤140	<5	2.0−20.0	0.0−6.0	≤10	≤1		noncarcinogenic
3a	332.36	0.97	55.68	99.53	83.25	1.78	5	1	5	0	high	noncarcinogenic
3b	408.45	0.98	61.78	100.00	74.46	3.15	5	0	6	0	high	noncarcinogenic
3c	498.45	0.90	50.86	99.39	166.12	1.47	9	0	8	1	low	noncarcinogenic
4a	392.41	0.83	51.72	98.24	101.71	1.18	7	1	7	0	high	noncarcinogenic
4b	468.50	0.87	53.48	99.66	92.92	2.50	7	0	8	0	high	noncarcinogenic
4c	558.50	0.80	50.00	99.26	184.66	0.92	11	0	10	2	low	noncarcinogenic
5a	375.42	0.88	57.66	99.13	86.49	1.70	5	1	6	0	high	noncarcinogenic
5b	451.52	0.94	62.83	100.00	77.70	3.02	5	0	7	0	high	noncarcinogenic
5c	541.51	0.74	51.45	99.29	169.36	1.39	9	0	9	2	low	noncarcinogenic
6a	348.36	0.79	55.60	98.95	103.48	1.25	6	2	5	0	high	noncarcinogenic
6b	424.45	0.89	53.85	100.00	94.69	2.61	6	1	6	0	high	noncarcinogenic
6c	514.45	0.73	52.45	99.13	186.35	0.99	10	1	8	2	high	noncarcinogenic
7a	377.35	0.85	50.75	95.12	129.07	0.90	7	1	6	0	high	noncarcinogenic
7b	453.45	0.90	50.86	99.39	120.28	2.27	7	0	7	0	high	noncarcinogenic
7c	543.44	0.90	50.86	99.39	211.94	0.72	11	0	9	2	low	noncarcinogenic
8a	358.39	0.97	55.68	99.53	83.25	2.16	5	1	6	0	high	noncarcinogenic
8b	434.49	0.98	61.78	100.00	74.46	3.48	5	0	7	0	high	noncarcinogenic
8c	524.48	0.90	50.86	99.31	166.12	1.81	9	0	9	2	low	noncarcinogenic
9a	401.46	0.88	57.66	99.13	86.49	2.07	5	1	7	0	high	noncarcinogenic
9b	477.56	0.94	62.83	100.00	77.70	3.35	5	0	8	0	high	noncarcinogenic
9c	567.55	0.74	51.45	99.29	169.36	1.72	9	0	10	2	low	noncarcinogenic

https://doi.org/10.1021/acsomega.2c02181
ACS Omega 2022, 7, 25265−25277

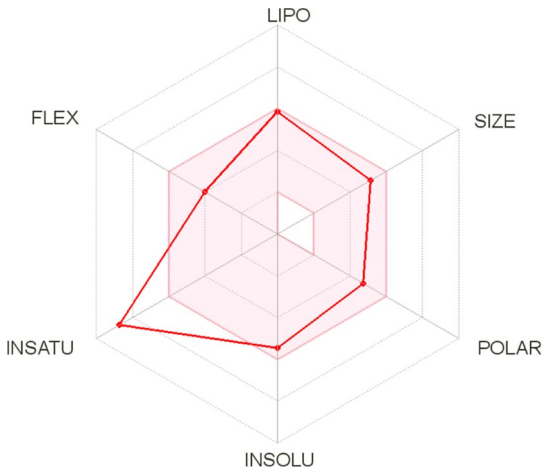

Figure 3. Oral bioavailability radar of the best compound **6b**.

representations of the best-docked compound **6b** intermolecular interactions with both targets. Compound **6b** docked to the protein PI3K through five H-bonds and two π-cation interactions with the amino acid residues Asn114, Val125, Cys126, Glu78, Ser690, Arg140, and Arg693 at distances of 2.99, 2.98, 2.95, 2.44, 2.71, 5.86, and 4.17, respectively (Table 2). In addition, compound **6b** interacted with the protein Akt through five H-bonds and one π-cation. The SAR study showed that heterocyclic rings as pyrazolinone and phenolic moieties in compound **6b** play a significant role for enhancing its activity.

Moreover, we performed further analysis for the compounds such as ADMET and drug-like properties, as represented in Table 3. The results suggested that the intestinal barrier may well absorb all compounds but not at the blood−brain barrier level. In addition, all compounds except **4c**, **5c**, **6c**, **7c**, **8c**, and **9c** obeyed the Lipinski rule of five (Ro5) by not having over one violation.

Conversely, the bioavailability radar (Figure 3) of the best-docked molecule **6b** showed that the pink-colored zone is the perfect space for each property. The plot suggested that compound **6b** could be a potential new anticancer drug candidate.

Antitumor/Cytotoxic (In Vitro) Studies. Compound **6b** was chosen from the molecular docking studies to investigate its potential as a new anticancer drug via inhibiting the PI3K/Akt and Raf-1/ERK1/2 signaling pathways. Compound **6b** showed significant antitumor effects on A549, MDA-231, Caco, PCL, and MCF-7 cancer cell lines with IC_{50} values equal to 40.91 ± 0.35, 38.45 ± 0.29, 23.34 ± 0.14, 56.33 ± 0.22, and 50.15 ± 0.14 μM, respectively. Our results showed that compound **6b** had more significant inhibitory effects on the Caco colon cancer cell line compared with DOX as a reference drug (IC_{50} = 6.713 ± 0.27 μM). Moreover, compound **6b** showed lower cytotoxic effects on WISH normal cells (IC_{50} = 124.4 ± 1.7 μM). This means that it is more powerful against cancer cell proliferation while having no damaging side effects on healthy cells; this is in line with the in silico results. DOX, on the other hand, has an extremely cytotoxic effect on normal cells (IC_{50} = 19.27 ± 0.31 μM) (Figure 4). Thus, the Caco cell line was selected for further analysis.

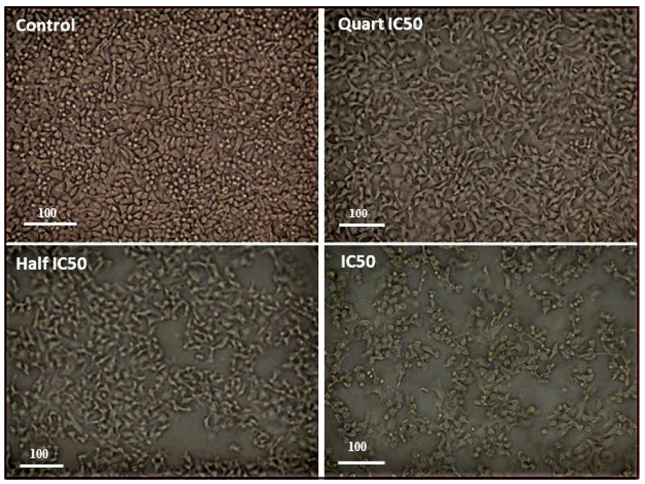

Figure 5. Morphological features of apoptosis in the Caco cells treated with compound **6b** in a dose-dependent manner (1/4IC_{50}, 1/2IC_{50}, IC_{50}) after 48 h treatment.

Alternation in Morphological Features. Cytotoxic agents infrequently alter the cell morphology, resulting in an abnormal cell morphology, increased cell debris, and decreased cell numbers. In the present study, detectable morphological features of apoptosis were observed in Caco cells treated with compound **6b** in a dose-dependent manner (1/4IC_{50}, 1/2IC_{50}, IC_{50}), including cellular shrinkage with the cell number reduced and detachment, cell rounding, and cytoplasmic condensation. However, the morphology of the untreated cells appeared normal and confluent, as shown in Figure 5. These results further elaborated the ability of compound **6b** in inducing apoptosis.

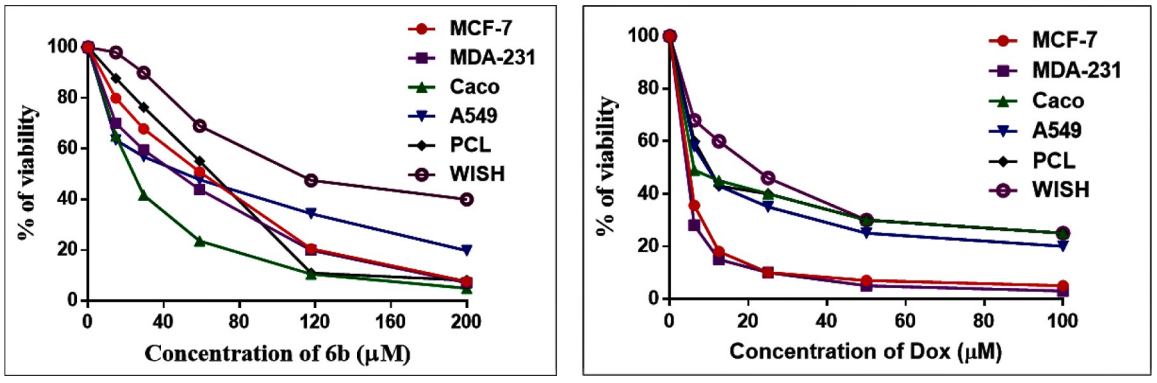

Figure 4. Antitumor/cytotoxic effect of compound **6b** and doxorubicin on various cell lines.

https://doi.org/10.1021/acsomega.2c02181
ACS Omega 2022, 7, 25265−25277

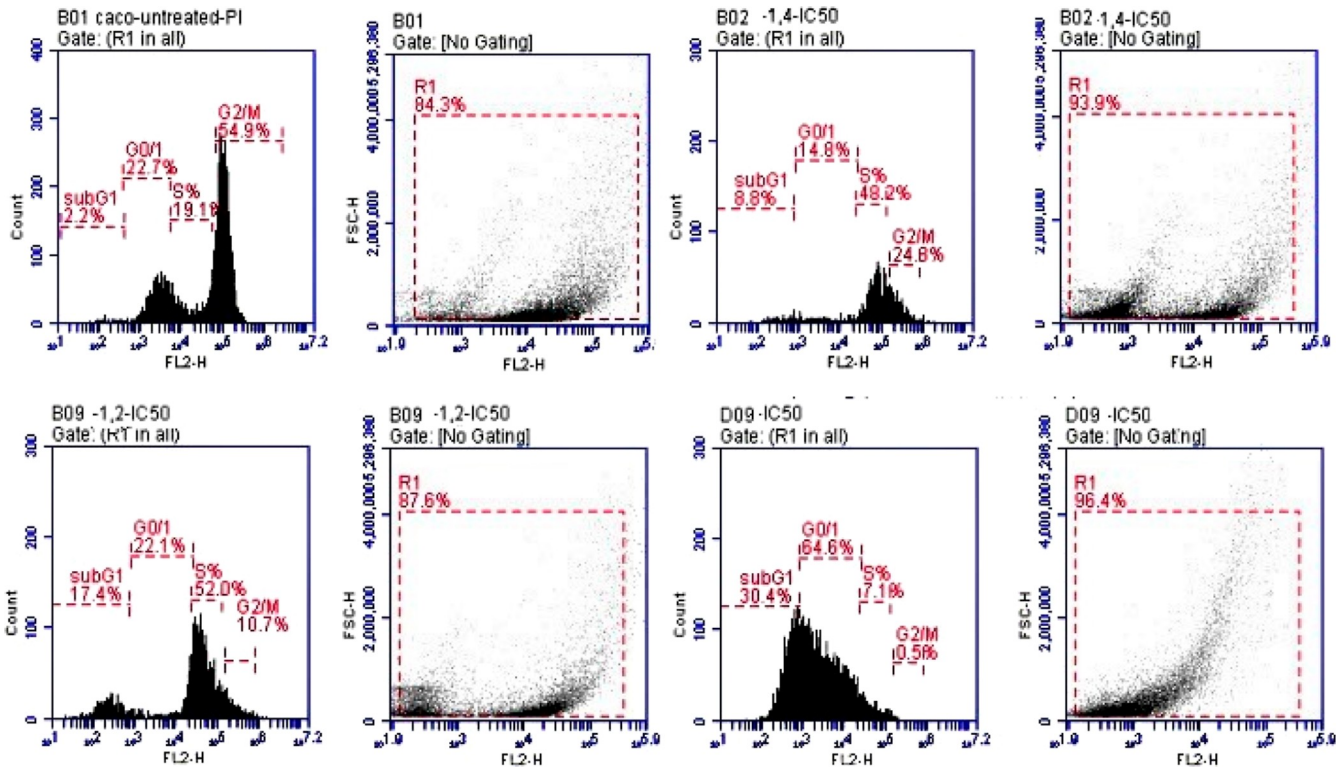

Figure 6. Cell cycle phases of compound **6b** in the Caco cell line in a dose-dependent manner ($1/4IC_{50}$, $1/2IC_{50}$, IC_{50}) after 48 h treatment.

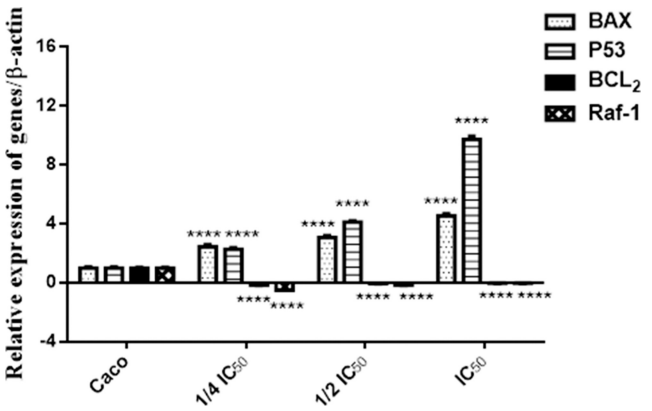

Figure 7. Relative expression of Raf-1, P53, Bax, and Bcl_{-2} in the Caco cell line (compound **6b**) in a dose-dependent manner ($1/4IC_{50}$, $1/2IC_{50}$, IC_{50}) after 48 h treatment.

Cell Cycle Arrest Detection. The inhibition of the PI3K/Akt protein kinases causes cell cycle arrest. Moreover, this arrest confirmed the reduction in proliferation and metastasis of the Caco cancer cell line via inhibiting the Raf-1/ERK1/2 signaling pathway. Compound **6b** enhanced the percentage of cells in the sub-G0/G1 phase in Caco cells at all doses when compared with the untreated cells (this is the phase in which cells wait to enter the cell cycle to duplicate; when the number of cells in this phase rises, the cell cycle has been stopped, and division and replication are impossible). The $1/4IC_{50}$, $1/2IC_{50}$, and IC_{50} of compound **6b** showed cell cycle arrest at rates of 8.8, 17.4, and 30.4%, respectively, in the sub-G_0/G_1 phase compared to untreated Caco cells (2.2%). This means that compound **6b** inhibits cell growth, arrest in cell cycle progression, and the increase of cells in G1 reflecting its apoptotic effect, and the G2/M checkpoint blocks the entry into mitosis when DNA is damaged, as illustrated in Figure 6.

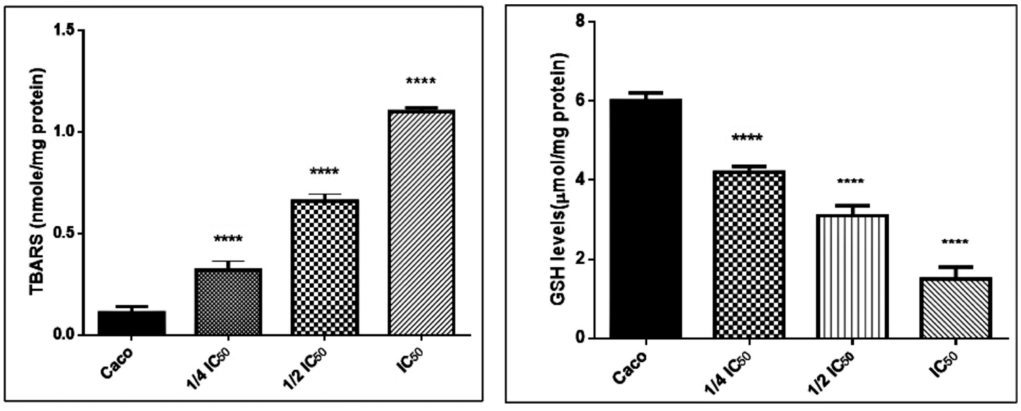

Figure 8. MDA and GSH levels in the Caco cell line (compound **6b**) in a dose-dependent manner ($1/4IC_{50}$, $1/2IC_{50}$, IC_{50}) after 48 h treatment.

https://doi.org/10.1021/acsomega.2c02181
ACS Omega 2022, 7, 25265−25277

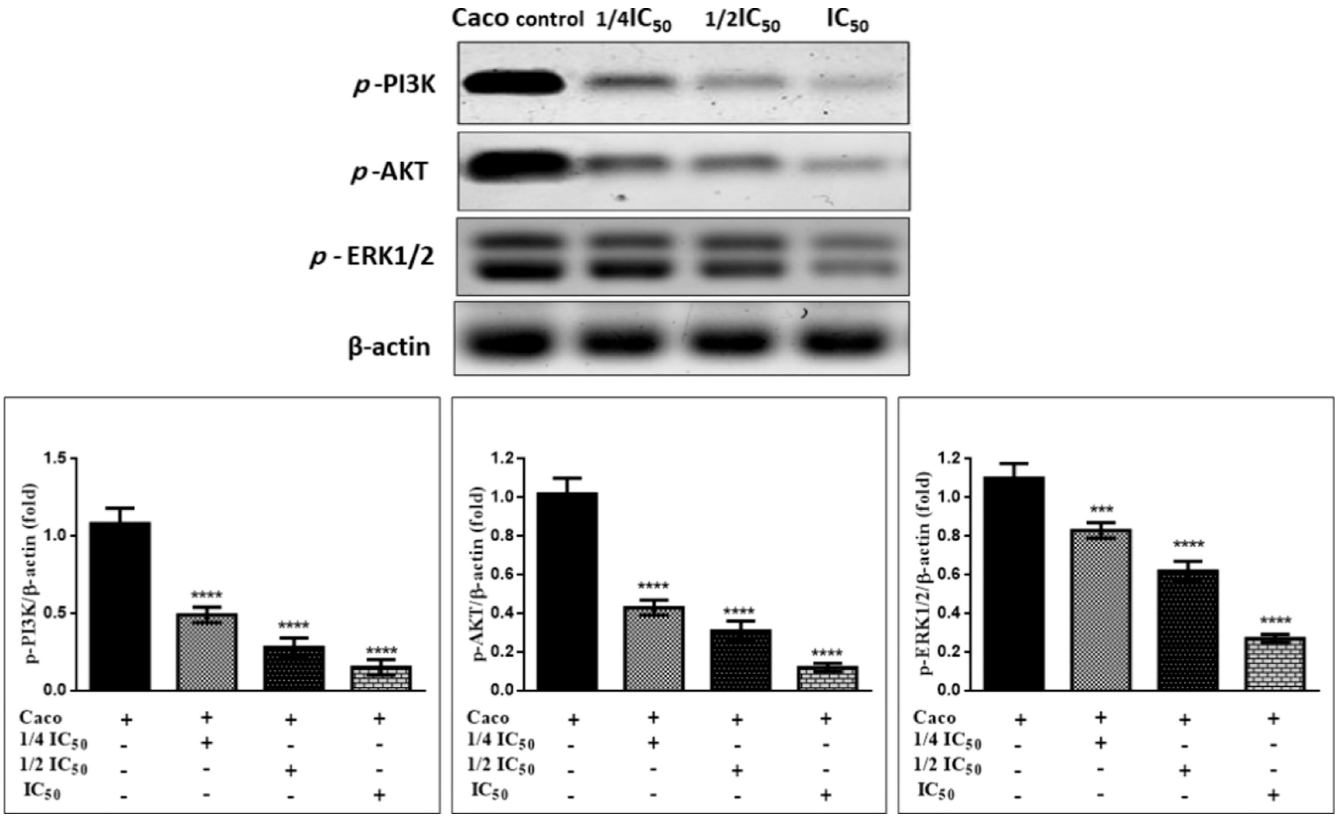

Figure 9. Effects of compound **6b** on the phosphorylation of PI3K/Akt/ERK1/2 in Caco cells. The cells were treated with the $1/4IC_{50}$, $1/2IC_{50}$, and IC_{50} for 48 h, and the protein phosphorylation levels were relative to β-actin protein (internal control) using western blot analysis.

Collectively, these results demonstrated that compound **6b** can induce inhibition to PI3K/Akt and Raf-1/ERK1/2 signaling pathways and trigger apoptosis via arresting the cell cycle in the sub-G_0/G_1 phase in a dose-dependent manner.[38,39]

qRT-PCR Study. qRT-PCR was used to measure the mRNA expression of the Bax, p53 (apoptotic markers), Bcl_{-2} (antiapoptotic marker), and Raf-1 (proliferative marker) genes in the Caco cell line. In cells treated with compound **6b**, the expression of Bax and p53 was considerably ($p < 0.0001$) increased in a dose-dependent manner, with the highest expression in the IC_{50} of cells treated with compound **6b** compared to untreated cells. Bcl_{-2} and Raf-1 gene expressions were dramatically ($p < 0.0001$) downregulated in compound **6b**-treated cells in a dose-dependent manner, with a little expression in the IC_{50} of compound **6b**-treated cells compared to untreated cells, as shown in Figure 7. As a result, the upregulation of Bax expression and downregulation of Bcl_{-2} expression indicate that compound **6b** causes mitochondrial membrane dysfunction that causes release of cytochrome C and activation of the caspase cascade that finally led to apoptosis. In contrast, the upregulation of p53 expression and downregulation of the expression of the proliferative gene Raf-1 result from the inhibition of PI3K/Akt and lead to inhibit ERK1/2 signaling pathways. This clarifies the ability of compound **6b** to inhibit cell proliferation, angiogenesis, and metastasis, leading to cell cycle arrest and apoptosis induction.[39,40]

Antioxidant/Oxidative Stress Biomarkers. Our results revealed that the level of MDA that results from the lipid peroxidation process occurring in Caco cells treated with compound **6b** in a dose-dependent manner ($1/4IC_{50}$, $1/2IC_{50}$, IC_{50}) was increased significantly, while the specific activity of reduced glutathione (GSH) was remarkably diminished as compared with the untreated Caco cells, as shown in Figure 8. This implies that compound **6b** could promote programming cell death in cancer cells by generating intracellular ROS and blocking the antioxidant endogenous enzymes. According to this theory, the high ROS production in cancer cells causes malfunction of the mitochondrial membrane, inhibits the PI3K/Akt protein kinase, and leads to the Raf-1/ERK1/2 signaling pathway inhibition. Finally, apoptosis is induced, and cell survival, proliferation, and metastasis are arrested.[38,41−43]

Immunoblotting Confirms the Inhibition of the PI3K/Akt/ERK1/2 Signaling Pathway. Our results elucidated that compound **6b** induces a remarkable drop in PI3K/Akt protein kinase with a significant decrease in ERK1/2 in the Caco colon cancer cell line dose-dependently as compared to untreated cells, Figure 9. These findings confirmed compound **6b**'s mechanical routes of inhibition of PI3K, which inhibits PIP3 and promotes ROS intracellular production, resulting in Akt inhibition via dephosphorylation. When Akt is dephosphorylated, p53 is activated due to blocking MDM2 protein and the cell cycle is stopped. Additionally, it inhibits Raf-1, which leads to inhibition of MEK protein and finally causes ERK1/2 inhibition, arresting cell proliferation, angiogenesis, and metastasis.[44−48]

CONCLUSIONS

The condensation of azo pyrazolinone derivatives with various aromatic aldehydes yielded a series of novel pyrazolinone chalcones **3**−**9**. This has been confirmed by spectroscopic techniques as well as elemental analyses. The newly

https://doi.org/10.1021/acsomega.2c02181
ACS Omega 2022, 7, 25265−25277

synthesized pyrazolinone chalcone (**6b**) was selected according to its in silico molecular binding energy toward PI3K/Akt protein kinases. Consequently, in vitro studies approved that the chosen compound **6b** causes apoptosis and cell death by inducing ROS generation-mediated inhibition of PI3K/Akt. The cellular mechanism of interdependence between PI3K/Akt inhibition and Raf-1/ERK1/2 proliferative inhibition, p53 activation, and cell cycle arrest involved in the Caco colon cancer cell line has been elucidated. According to our results, compound **6b** could be used as a promising anticancer agent.

■ ASSOCIATED CONTENT

Supporting Information

The Supporting Information is available free of charge at https://pubs.acs.org/doi/10.1021/acsomega.2c02181.

Spectral data for all compounds and docking and biological studies (PDF)

■ AUTHOR INFORMATION

Corresponding Author

Aboubakr H. Abdelmonsef − *Chemistry Department, Faculty of Science, South Valley University, Qena 83523, Egypt;* orcid.org/0000-0002-4616-0224; Email: aboubakr.ahmed@sci.svu.edu.eg

Authors

Ahmed A. Noser − *Organic Chemistry, Chemistry Department, Faculty of Science, Tanta University, Tanta 31527, Egypt*

Ihsan A. Shehadi − *Department of Chemistry, Pure and Applied Chemistry Research Group, College of Sciences, University of Sharjah, Sharjah 27272, UAE*

Maha M. Salem − *Biochemistry Division, Chemistry Department, Faculty of Science, Tanta University, Tanta 31527, Egypt*

Complete contact information is available at: https://pubs.acs.org/10.1021/acsomega.2c02181

Author Contributions

A.A.N., I.A.S., A.H.A., and M.M.S contributed in this work

Funding

This research received no external funding.

Notes

The authors declare no competing financial interest.

■ ACKNOWLEDGMENTS

This in vitro study was conducted in the Center of Excellence for Research in Regenerative Medicine and Its Applications (CERRMA), Faculty of Medicine, Alexandria University, Egypt.

■ REFERENCES

(1) Abu-Khudir, R.; Ismail, G. A.; Diab, T. Antimicrobial, antioxidant, and anti-tumor activities of Sargassum linearifolium and Cystoseira crinita from Egyptian Mediterranean Coast. *Nutr. Cancer* **2021**, *73*, 829−844.

(2) von Meyenfeldt, M. Cancer-associated malnutrition: An introduction. *Eur. J. Oncol. Nurs.* **2005**, *9*, S35−S38.

(3) Noser, A. A.; El-Naggar, M.; Donia, T.; Abdelmonsef, A. H. Synthesis, In Silico and In Vitro Assessment of New Quinazolinones as Anticancer Agents via Potential AKT Inhibition. *Molecules* **2020**, *25*, 4780.

(4) Wang, X.; Li, R.; Zhao, X.; Yu, X.; Sun, Q. Metformin Promotes HaCaT Cell Apoptosis through Generation of Reactive Oxygen Species via Raf-1-ERK1/2-Nrf2 Inactivation. *Inflammation* **2018**, *41*, 948−958.

(5) An, W.; et al. Apoptotic pathway as the therapeutic target for anticancer traditional Chinese medicines. *Front. Pharmacol.* **2019**, *10*, 758.

(6) Braicu, C.; et al. A Comprehensive Review on MAPK: A Promising Therapeutic Target in Cancer. *Cancers* **2019**, *11*, 1618.

(7) Naim, M. J.; Alam, O.; Nawaz, F.; Alam, M. J.; Alam, P. Current status of pyrazole and its biological activities. *J. Pharm. BioAllied Sci.* **2016**, *8*, 2−17.

(8) Ouyang, Y.; et al. Chalcone derivatives: Role in anticancer therapy. *Biomolecules* **2021**, *11*, 894.

(9) Matthee, C.; Terre'Blanche, G.; Legoabe, L. J.; Janse van Rensburg, H. D. Exploration of chalcones and related heterocycle compounds as ligands of adenosine receptors: therapeutics development. *Mol. Diversity* **2021**, DOI: 10.1007/s11030-021-10257-9.

(10) Elkhalifa, D.; Al-Hashimi, I.; Al Moustafa, A.-E.; Khalil, A. A comprehensive review on the antiviral activities of chalcones. *J. Drug Target.* **2021**, *29*, 403−419.

(11) Tong, Y.; Lyu, Y.; Xu, S.; Zhang, L.; Zhou, J. Optimum chalcone synthase for flavonoid biosynthesis in microorganisms. *Crit. Rev. Biotechnol.* **2021**, *41*, 1194−1208.

(12) Farooq, S.; Ngaini, Z. One-pot and two-pot synthesis of chalcone based mono and bis-pyrazolines. *Tetrahedron Lett.* **2020**, *61*, 151416.

(13) Ozmen Ozgun, D.; Gul, H. I.; Yamali, C.; Sakagami, H.; Gulcin, I.; Sukuroglu, M.; Supuran, C. T. Synthesis and bioactivities of pyrazoline benzensulfonamides as carbonic anhydrase and acetylcholinesterase inhibitors with low cytotoxicity. *Bioorg. Chem.* **2019**, *84*, 511−517.

(14) Haider, K.; Shafeeque, M.; Yahya, S.; Yar, M. S. A comprehensive review on pyrazoline based heterocyclic hybrids as potent anticancer agents. *Eur. J. Med. Chem. Rep.* **2022**, *5*, 100042.

(15) Alharthy, R. D. Design and Synthesis of Novel Pyrazolo[3,4-d]Pyrimidines: In Vitro Cytotoxic Evaluation and Free Radical Scavenging Activity Studies. *Pharm. Chem. J.* **2020**, *54*, 273−278.

(16) Khalil, A.; Hassan, M.; Mohamed, M.; Elsayed, A. Metal salt-catalyzed diazocoupling of 3-substituted-1-pyrazol-2-in-5-ones in aqueous medium. *Dyes Pigm.* **2005**, *66*, 241−245.

(17) Rashdan, H. R. M.; Shehadi, I. A.; Abdelmonsef, A. H. Synthesis, Anticancer Evaluation, Computer-Aided Docking Studies, and ADMET Prediction of 1,2,3-Triazolyl-Pyridine Hybrids as Human Aurora B Kinase Inhibitors. *ACS Omega* **2021**, *6*, 1445−1455.

(18) Rashdan, H. R. M.; Abdelmonsef, A. H.; Abou-Krisha, M. M.; Yousef, T. A. Synthesis, Identification, Computer-Aided Docking Studies, and ADMET Prediction of Novel Benzimidazo-1,2,3-triazole Based Molecules as Potential Antimicrobial Agents. *Molecules* **2021**, *26*, 7119.

(19) Abdelmonsef, A. H.; Mosallam, A. M. Synthesis, in vitro biological evaluation and in silico docking studies of new quinazolin-2,4-dione analogues as possible anticarcinoma agents. *J. Heterocycl. Chem.* **2020**, *57*, 1637−1654.

(20) Abo-Bakr, A. M.; Alsoghier, H. M.; Abdelmonsef, A. H. Molecular Docking, Modeling, Semiempirical Calculations Studies and In Vitro Evaluation of New Synthesized Pyrimidin-imide Derivatives. *J. Mol. Struct.* **2022**, *1249*, 131548.

(21) Abdelmonsef, A. H.; et al. A search for antiinflammatory therapies: Synthesis, in silico investigation of the mode of action, and in vitro analyses of new quinazolin-2,4-dione derivatives targeting phosphodiesterase-4 enzyme. *J. Heterocycl. Chem.* **2022**, *59*, 474−492.

(22) Haredi Abdelmonsef, A.; Eldeeb Mohamed, M.; El-Naggar, M.; Temairk, H.; Mohamed Mosallam, A. Novel Quinazolin-2,4-Dione Hybrid Molecules as Possible Inhibitors Against Malaria: Synthesis and in silico Molecular Docking Studies. *Front. Mol. Biosci.* **2020**, *7*, 105.

(23) Shehadi, I. A.; Rashdan, H. R. M.; Abdelmonsef, A. H. Homology Modeling and Virtual Screening Studies of Antigen

MLAA-42 Protein: Identification of Novel Drug Candidates against Leukemia-An In Silico Approach. *Comput. Math. Methods Med.* **2020**, *2020*, 8196147.
(24) Haredi Abdelmonsef, A. Computer-aided identification of lung cancer inhibitors through homology modeling and virtual screening. *Egypt. J. Med. Hum. Genet.* **2019**, *20*, 6.
(25) Berman, H. M.; et al. The protein data bank. *Nucleic Acids Res.* **2000**, *28*, 235−242.
(26) Brooks, B. R.; et al. CHARMM: Molecular dynamics simulation package. *J. Comput. Chem.* **2009**, *30*, 1545−1614.
(27) O'Boyle, N. M.; et al. Open Babel: An Open chemical toolbox. *J. Cheminf.* **2011**, *3*, 33.
(28) Rappé, A. K.; Casewit, C. J.; Colwell, K. S.; Goddard, W. A.; Skiff, W. M. UFF, a Full Periodic Table Force Field for Molecular Mechanics and Molecular Dynamics Simulations. *J. Am. Chem. Soc.* **1992**, *114*, 10024−10035.
(29) Dallakyan, S.; Olson, A. J. Small-Molecule Library Screening by Docking with PyRx. *Chemical Biology*; Springer, 2015; Vol. *1263*, pp 243−250.
(30) Dash, S. K.; Ghosh, T.; Roy, S.; Chattopadhyay, S.; Das, D. Zinc sulfide nanoparticles selectively induce cytotoxic and genotoxic effects on leukemic cells: Involvement of reactive oxygen species and tumor necrosis factor alpha. *J. Appl. Toxicol.* **2014**, *34*, 1130−1144.
(31) Noser, A. A.; Abdelmonsef, A. H.; El-naggar, M.; Salem, M. M. New Amino Acid Schiff Bases as Anticancer Agents via Potential Mitochondrial Complex I-Associated Hexokinase Inhibition and Targeting AMP-Protein Kinases/mTOR Signaling Pathway. *Molecules* **2021**, *26*, 5332.
(32) Darzynkiewicz, Z.; Halicka, H. D.; Zhao, H. Analysis of Cellular DNA Content by Flow and Laser Scanning Cytometry. *Polyploidization and Cancer. Advances in Experimental Medicine and Biology*; Poon, R. Y. C., Ed.; Springer: New York, 2010; pp 137−147
(33) Kvastad, L.; et al. Single cell analysis of cancer cells using an improved RT-MLPA method has potential for cancer diagnosis and monitoring. *Sci. Rep.* **2015**, *5*, 16519.
(34) Livak, K. J.; Schmittgen, T. D. Analysis of relative gene expression data using real-time quantitative PCR and the 2-ΔΔCT method. *Methods* **2001**, *25*, 402−408.
(35) Salem, M. M.; et al. Propolis Potentiates Methotrexate Anticancer Mechanism and Reduces its Toxic Effects. *Nutr. Cancer* **2020**, *72*, 460−480.
(36) Bradford, M. M. A rapid and sensitive method for the quantitation of microgram quantities of protein utilizing the principle of protein-dye binding. *Anal. Biochem.* **1976**, *72*, 248−254.
(37) Mruk, D. D.; Cheng, C. Y. Enhanced chemiluminescence (ECL) for routine immunoblotting. *Spermatogenesis* **2011**, *1*, 121−122.
(38) Liu, Y.; et al. Inhibition of PI3K/AKT signaling via ROS regulation is involved in rhein-induced apoptosis and enhancement of oxaliplatin sensitivity in pancreatic cancer cells. *Int. J. Biol. Sci.* **2021**, *17*, 589−602.
(39) Lim, W.; Song, G. Inhibitory effects of delphinidin on the proliferation of ovarian cancer cells via PI3K/AKT and ERK 1/2 MAPK signal transduction. *Oncol. Lett.* **2017**, *14*, 810−818.
(40) McCubrey, J. A.; et al. Roles of the Raf/MEK/ERK pathway in cell growth, malignant transformation and drug resistance. *Biochim. Biophys. Acta, Mol. Cell Res.* **2007**, *1773*, 1263−1284.
(41) Wen, C.; et al. ROS-mediated inactivation of the PI3K/AKT pathway is involved in the antigastric cancer effects of thioredoxin reductase-1 inhibitor chaetocin. *Cell Death Dis.* **2019**, *10*, 809.
(42) Mishra, R.; et al. Phosphoinositide 3-kinase (Pi3k) reactive oxygen species (ros)-activated prodrug in combination with anthracycline impairs pi3k signaling, increases dna damage response and reduces breast cancer cell growth. *Int. J. Mol. Sci.* **2021**, *22*, 2088.
(43) Kang, X.; et al. Alantolactone induces apoptosis through ROS-mediated AKT pathway and inhibition of PINK1-mediated mitophagy in human HepG2 cells. *Artif. Cells, Nanomed., Biotechnol.* **2019**, *47*, 1961−1970.
(44) Yao, W.; et al. Delicaflavone induces ROS-mediated apoptosis and inhibits PI3K/AKT/mTOR and Ras/MEK/Erk signaling pathways in colorectal cancer cells. *Biochem. Pharmacol.* **2020**, *171*, 113680.
(45) Su, X.; et al. Vitamin C kills thyroid cancer cells through ROS-dependent inhibition of MAPK/ERK and PI3K/AKT pathways via distinct mechanisms. *Theranostics* **2019**, *9*, 4461−4473.
(46) Wang, X.; et al. ROS Promote ox-LDL-induced platelet activation by up-regulating autophagy through the inhibition of the PI3K/AKT/mTOR pathway. *Cell. Physiol. Biochem.* **2018**, *50*, 1779−1793.
(47) Deng, S.; et al. Dexamethasone induces osteoblast apoptosis through ROS-PI3K/AKT/GSK3β signaling pathway. *Biomed. Pharmacother.* **2019**, *110*, 602−608.
(48) Gao, X.; et al. Cocoa tea (Camellia ptilophylla) induces mitochondria-dependent apoptosis in HCT116 cells via ROS generation and PI3K/Akt signaling pathway. *Food Res. Int.* **2020**, *129*, 108854.

https://doi.org/10.1021/acsomega.2c02181
ACS Omega 2022, 7, 25265−25277